Title
The Early 1990s Change in ENSO–PSA–SAM Relationships and Its Impact on Southern Hemisphere Climate

Journal
Journal of Climate, 28(23)

ISSN
0894-8755

Authors
Yu, Jin-Yi
Paek, Houk
Saltzman, Eric S
et al.

Publication Date
2015-12-01

DOI
10.1175/jcli-d-15-0335.1

SPECIAL
Connecting the Tropics to the Polar Regions
COLLECTION

The Early 1990s Change in ENSO–PSA–SAM Relationships and Its Impact on Southern Hemisphere Climate

JIN-YI YU, HOUK PAEK, AND ERIC S. SALTZMAN

Department of Earth System Science, University of California, Irvine, Irvine, California

TONG LEE

Jet Propulsion Laboratory, California Institute of Technology, Pasadena, California

(Manuscript received 10 May 2015, in final form 1 September 2015)

ABSTRACT

This study uncovers an early 1990s change in the relationships between El Niño–Southern Oscillation (ENSO) and two leading modes of the Southern Hemisphere (SH) atmospheric variability: the southern annular mode (SAM) and the Pacific–South American (PSA) pattern. During austral spring, while the PSA maintained a strong correlation with ENSO throughout the period 1948–2014, the SAM–ENSO correlation changed from being weak before the early 1990s to being strong afterward. Through the ENSO connection, PSA and SAM became more in-phase correlated after the early 1990s. The early 1990s is also the time when ENSO changed from being dominated by the eastern Pacific (EP) type to being dominated by the central Pacific (CP) type. Analyses show that, while the EP ENSO can excite only the PSA, the CP ENSO can excite both the SAM and PSA through tropospheric and stratospheric pathway mechanisms. The more in-phase relationship between SAM and PSA impacted the post-1990s Antarctic climate in at least two aspects: 1) a stronger Antarctic sea ice dipole structure around the Amundsen–Bellingshausen Seas due to intensified geopotential height anomalies over the region and 2) a shift in the phase relationships of surface air temperature anomalies among East Antarctica, West Antarctica, and the Antarctic Peninsula. These findings imply that ENSO–Antarctic climate relations depend on the dominant ENSO type and that ENSO forcing has become more important to the Antarctic sea ice and surface air temperature variability in the past two decades and will in the coming decades if the dominance of CP ENSO persists.

1. Introduction

The linkages between the Southern Hemisphere (SH) climate and the tropical Pacific sea surface temperatures (SSTs), particularly those associated with El Niño–Southern Oscillation (ENSO), have been extensively studied (e.g., Karoly 1989; Mo 2000; Yuan 2004; Fogt and Bromwich 2006; L'Heureux and Thompson 2006; Lee et al. 2010). Two leading modes of SH atmospheric variability have been often emphasized: the southern annular mode (SAM; Hartmann and Lo 1998; Thompson and Wallace 2000) and the Pacific–South American (PSA; Mo and Ghil 1987) pattern. The SAM is characterized by out-of-phase sea level pressure (SLP) variations between midlatitudes (~40°S) and high latitudes (~65°S). Previous studies have suggested that the SAM is generated primarily by the internal dynamics of the SH atmosphere, which involves eddy–mean flow interactions (e.g., Yu and Hartmann 1993; Feldstein and Lee 1998; Hartmann and Lo 1998; Limpasuvan and Hartmann 2000; Lorenz and Hartmann 2001). Forcing from the tropics, such as that associated with ENSO, is considered less important, although correlations can be found between SAM and ENSO in austral summer (e.g., Karoly 1989; Seager et al. 2003; Silvestri and Vera 2003; Zhou and Yu 2004; Codron 2005; L'Heureux and Thompson 2006). The PSA is characterized by a stationary Rossby wave train emanating from the tropical central Pacific with major anomaly centers to the east of New Zealand, in the Amundsen–Bellingshausen Seas, and near the southern tip of South America. The positive phase of the PSA is known to be related to La Niña and the negative phase of the PSA is related to El Niño (e.g., Mo 2000). Previous studies showed that ENSO, together with various phases of the SAM and the PSA, can influence the Southern

Corresponding author address: Dr. Jin-Yi Yu, Department of Earth System Science, University of California, Irvine, 3200 Croul Hall St., Irvine, CA 92697-3100.
E-mail: jyyu@uci.edu

DOI: 10.1175/JCLI-D-15-0335.1

Ocean SSTs (e.g., Ciasto and Thompson 2008; Lee et al. 2010; Yeo and Kim 2015), Antarctic sea ice concentrations (e.g., Liu et al. 2004; Stammerjohn et al. 2008; Yuan and Li 2008), and Antarctic surface air temperatures (e.g., Kwok and Comiso 2002; Ding et al. 2011).

Fogt and Bromwich (2006) found that the ENSO influences on the SH strengthened from the 1980s to the 1990s. They noted that the ENSO-excited PSA became more in phase with the SAM in the 1990s to give rise to a stronger ENSO influence. Their study indicates that the relationships among ENSO, PSA, and SAM can change from decade to decade. Interestingly, the early 1990s is the time when ENSO changed from being mostly of the eastern Pacific (EP) type to the central Pacific (CP) type (Yu et al. 2012a, 2015). This early 1990s change in ENSO properties is a possible reason for the change in ENSO–SH climate relationships. The terms CP ENSO and EP ENSO were introduced by Yu and Kao (2007) and Kao and Yu (2009) to emphasize the different longitudinal positions of these types of ENSO. The EP ENSO is the conventional type of ENSO similar to that portrayed by Rasmusson and Carpenter (1982), which typically onsets and develops near the South American coast and has its SST anomalies centered in the equatorial eastern Pacific. The CP ENSO tends to onset, develop, and decay locally in the equatorial central Pacific. There are indications that the shift in the longitudinal position of ENSO SST variability in recent decades may change the ENSO impacts on the SH climate. For example, Lee et al. (2010) argued that the 2009/10 CP El Niño event caused a record-breaking warming in the South Pacific and western Antarctica associated with a strong anticyclone in the region. Ding et al. (2011) also suggested that the substantial warming in West Antarctica in the recent decades is related to the warming trend of SST in the tropical central Pacific through an enhanced anticyclone over the Amundsen Sea. Lee and McPhaden (2010) suggested that the more frequent occurrence of CP El Niño has contributed to the SST warming trend in the tropical central Pacific. Several recent studies have begun to examine the possible different impacts of the two types of ENSO on the SH climate using observations (Hurwitz et al. 2011; Song et al. 2011; Sun et al. 2013; Ciasto et al. 2015) and model simulations (Zubiaurre and Calvo 2012; Hurwitz et al. 2013; Lim et al. 2013; Wilson et al. 2014).

In this study, we use observational and reanalysis datasets to examine if and specifically how the early 1990s change of ENSO type affects the relationships among ENSO, PSA, and SAM and how these changing relationships impact SH climate variability. We also examine how the two types of ENSO affect the relative importance of two mechanisms suggested to transmit ENSO forcing to high-latitude Southern Hemisphere: 1) an eddy–mean flow interaction mechanism in which an El Niño–induced intensification of the Hadley circulation and equatorward shift in the subtropical jet influence the propagation of midlatitude transient eddies and their associated eddy–mean flow interactions to give rise to a negative phase of the SAM (e.g., Seager et al. 2003) and 2) a stratospheric pathway mechanism in which El Niño events affect the propagation of planetary waves into the stratosphere and induce polar temperature and vortex anomalies that subsequently descend into the troposphere to excite the SAM (e.g., Mechoso et al. 1985; Hurwitz et al. 2011; Son et al. 2013; Evtushevsky et al. 2015). Here, we focus on the austral spring season [September–November (SON)] when ENSO–SH teleconnections are strongest (e.g., Jin and Kirtman 2009), the warming in West Antarctica is most significant (e.g., Schneider et al. 2012; Bromwich et al. 2013), and the maximum stratosphere–troposphere coupling occurs (Son et al. 2013).

This paper is organized as follows. Section 2 describes the datasets used in the study. Section 3 examines decadal variations in the relationships among ENSO, PSA, and SAM. Section 4 investigates the linkages between the two SH circulation modes and the two ENSO types. Section 5 discusses the mechanisms enabling the different types of ENSO to influence the SH climate, followed by a discussion of the changing ENSO impacts on SH climate in section 6. Conclusions are presented in section 7.

2. Datasets

In this study, the following datasets are used: 1) 500-hPa geopotential heights (Z500), zonal and meridional winds, and air temperatures from the National Centers for Environmental Prediction–National Center for Atmospheric Research (NCEP–NCAR) reanalysis dataset (Kalnay et al. 1996), and 2) the SST and sea ice concentrations from the Hadley Centre Sea Ice and Sea Surface Temperature dataset (HadISST; Rayner et al. 2003). The analyses focused primarily on the period 1948–2014. For sea ice concentrations, however, the data were available only during 1979–2014. Monthly anomalies were obtained by removing the mean seasonal cycles and linear trends.

3. Decadal variations in the relationships among ENSO, PSA, and SAM

To identify the SAM and PSA, we applied an empirical orthogonal function (EOF) analysis to the covariance matrix of the area-weighted monthly Z500 anomalies over 0°–90°S following Mo (2000). The two leading EOF

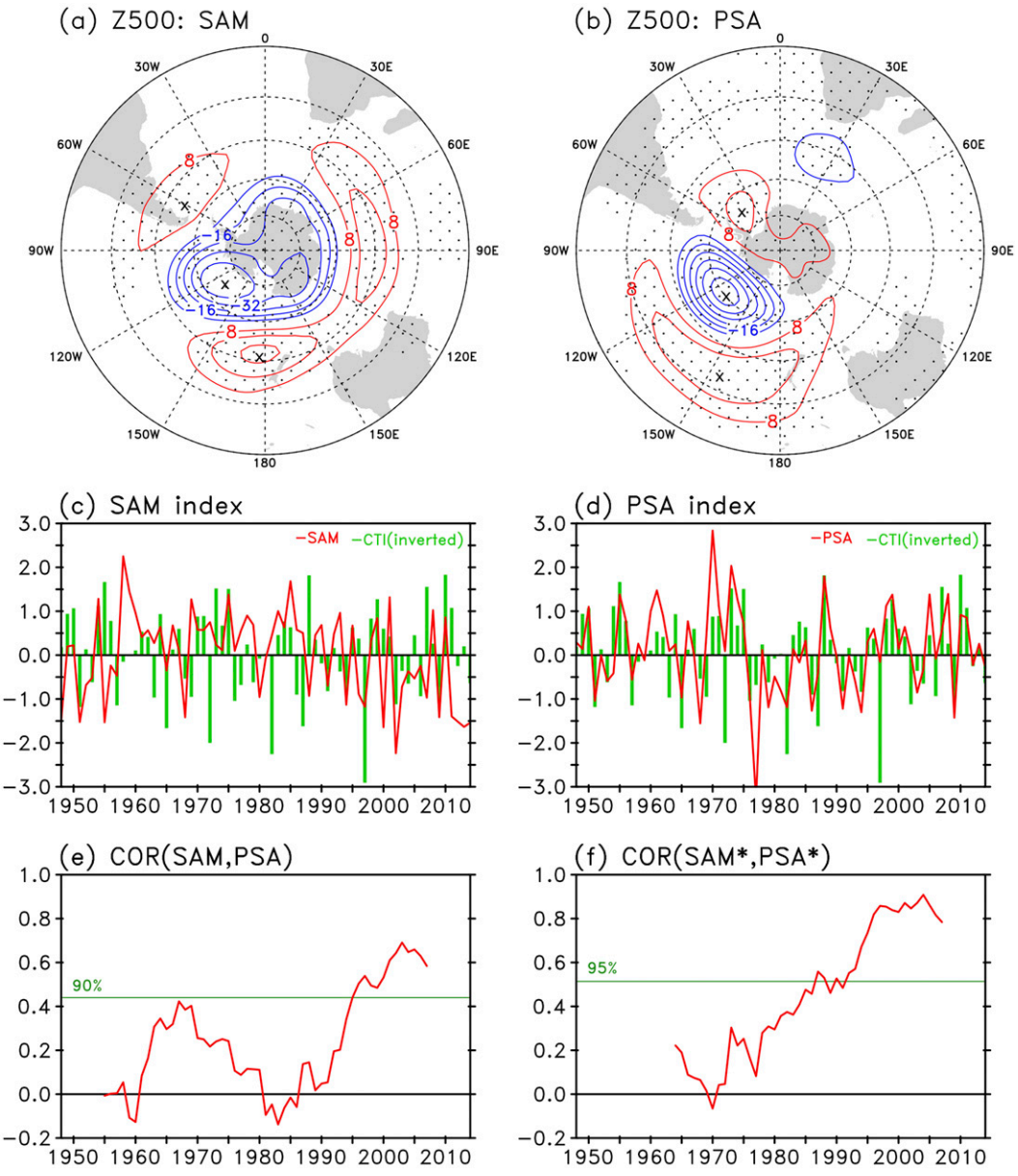

FIG. 1. (top) The Z500 anomaly structures of the (a) SAM and (b) PSA in austral spring (SON). Dots indicate areas where the values exceed the 95% confidence interval using a two-tailed Student's *t* test. Crosses mark the anomaly centers. Contours intervals are 8 m. (middle) The time series of (c) the SAM index and (d) the PSA index (red lines) with the inverted standardized CTI (green bars) superimposed. (bottom) The 15-yr running correlation coefficients (red lines) (e) between SAM and PSA indices and (f) between SAM* and PSA* indices. Green lines indicate the confidence intervals using a two-tailed Student's *t* test. The definition of SAM* and PSA* are given in the text.

modes, which account for 22% and 12% of the total variance, are the SAM and PSA, respectively. The corresponding standardized principal components (PCs) are referred to as the SAM and PSA indices, and their austral spring (SON) values averaged from the monthly PCs are shown in Figs. 1c and 1d. Similar EOFs and PCs were obtained by repeating the EOF analyses using subperiods of the entire data record of 1948–2014 (not shown). In the rest of the study, only the spring SAM and PSA indices are used in the analyses unless stated otherwise. The spatial patterns of these two modes are shown in Figs. 1a and 1b by regressing Z500 anomalies onto the SAM and PSA indices. The positive phase of the SAM (Fig. 1a) is characterized by a zonally symmetric structure that has negative height anomalies over the polar region (~60°–90°S) and positive anomalies at

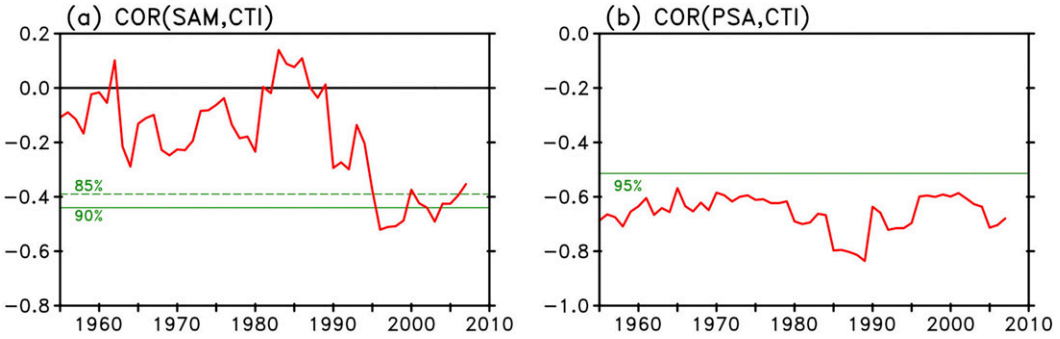

FIG. 2. The 15-yr running correlation coefficients (red lines) between the CTI and (a) the SAM index and (b) the PSA index. Green lines indicate statistical confidence intervals using a two-tailed Student's *t* test.

the midlatitudes (~30°–45°S) in both the Western and Eastern Hemispheres. In contrast, the positive phase of the PSA (Fig. 1b) is characterized by a zonally asymmetric structure that has a positive height anomaly center to the east of New Zealand (35°S, 152.5°W), a negative center in the Amundsen–Bellingshausen Seas (60°S, 126.5°W), and another positive center in the South American–Atlantic sector (65°S, 45°W). The PSA anomalies are located mostly in the Western Hemisphere and are very small in the Eastern Hemisphere. The SAM and PSA share three anomaly centers (at 47.5°S, 175°W; 67.5°S, 125°W; and 50°S, 60°W) in the South Pacific and Atlantic sectors. Various phase relationships between SAM and PSA can result in different impacts on SH climate. For example, an in-phase relationship can result in strong height anomalies over the Amundsen–Bellingshausen Seas by a superposition of the SAM and PSA anomalies.

To investigate the decadal variations in the PSA–SAM relationship, we calculated the running correlation coefficient between the SAM and PSA indices using a 15-yr moving window. As shown in Fig. 1e, the correlation coefficient was small during the 1960s–70s and weakened further in the 1980s, but dramatically increased to large positive values after the early 1990s. The correlation after the early 1990s is statistically significant at the 90% interval using a two-tailed Student's *t* test. To make sure that the early 1990s increase in correlation coefficient is not a result of the specific method used to construct the SAM and PSA indices, we repeated the running correlation analysis using alternative SAM and PSA indices (hereinafter SAM* and PSA*, respectively) that were defined by other authors. Following Marshall (2003), the SAM* index is defined as the difference of the zonal-mean SLP between 40° and 65°S based on observations from 12 weather stations. Following Yuan and Li (2008), the PSA* index is defined as the weighted average of Z500 anomalies at three specific locations (referred to as Z1, Z2, and Z3) in the following way: PSA* = (Z1 + Z2 − Z3)/3. Here, Z1 is located at 50°S, 45°W, Z2 is at 45°S, 170°W, and Z3 is at 67.5°S, 120°W. Figure 1f shows the running correlation coefficient between the SAM* and PSA* indices. The correlation was relatively small in the 1960s–80s but increased to large and significant values after the early 1990s. Both sets of indices show that the PSA and SAM became more in phase in SON after the early 1990s. Such an early 1990s shift in the PSA–SAM correlation was not found in the other seasons (not shown).

We next examined the decadal variations in the relationships between these two SH variability modes and ENSO. We used the cold tongue index (CTI; SST anomalies averaged over 6°S–6°N and 180°–90°W) to represent ENSO. The CTI domain covers both the tropical eastern and central Pacific and, therefore, can reflect the activity of both the EP and CP ENSOs. By superimposing the inverted CTI (green bars) onto the SAM and PSA indices (red lines) in Figs. 1c and 1d, we notice that the SAM index and CTI (Fig. 1c) do not show an obvious correlation before the early 1990s, but are correlated afterward. As for the PSA index (Fig. 1d), its variation seems to be more in phase with the variation of the CTI throughout the analysis period. These impressions are confirmed by Fig. 2, which shows the 15-yr running correlation coefficients between the CTI and the SAM and PSA indices. The CTI correlation with SAM (Fig. 2a) was weak during the 1960s–80s but significant (correlation coefficients around −0.5) after the early 1990s. The CTI correlation with PSA (Fig. 2b) was significant throughout the analysis period (correlation coefficients around −0.7), consistent with the suggestion that the PSA is excited primarily by ENSO forcing (e.g., Mo 2000). These analyses indicate that the ENSO forcing excited the PSA throughout the past seven decades, but did not become important for SAM until the early 1990s. The in-phase relationship between SAM and PSA in recent decades is likely a result of the increasing contribution of the ENSO forcing to the SAM

after the early 1990s. It should be pointed out that the third EOF mode of the Z500 anomalies (not shown) is characterized by a wave train pattern similar to the PSA except for a quadrature phase shift. This EOF mode is often referred to as the PSA2 (Mo 2000; Mo and Paegle 2001) and was suggested to be also excited by tropical convection (e.g., Mo and Higgins 1998; Mo and Paegle 2001) or as a mode of midlatitude intrinsic variability that resembles the PSA pattern (Robertson and Mechoso 2003; Zamboni et al. 2012). We repeated the correlation analyses presented in Figs. 1e and 2b with the PSA2 (not shown) and found the correlation coefficients failed to exceed the 90% confidence intervals. Therefore, the PSA2 is less associated with the SAM and ENSO and is not considered further in this study.

ENSO changed from the EP type to the CP type around the early 1990s (Yu et al. 2012a, 2015). To explore the influence of this change on the ENSO–PSA–SAM relationships, we examined the correlation between tropical SST anomalies with the spring SAM or PSA index for the period before the early 1990s (i.e., 1973–93; pre-1993 period hereinafter) and for the period after the early 1990s (1994–2014; post-1993 period hereinafter). During the pre-1993 period (Fig. 3a), the spring SAM index was not correlated with the tropical SST anomalies, which is consistent with the weak CTI–SAM correlations for that period (Fig. 2a). However, during the post-1993 period (Fig. 3b), negative correlations (90% confidence interval) occur in the tropical central Pacific from May of the El Niño developing year to the following February. The correlations appear first in the northeastern subtropical Pacific in late fall (i.e., May) and later spread toward the tropical central Pacific in winter (i.e., June–August). The strong correlations in the central Pacific grow and persist in the following spring and summer seasons (i.e., September–February). These SST correlations resemble the spatial structure and temporal evolution of the CP ENSO described in Kao and Yu (2009). For the PSA (Figs. 3c and 3d), significant correlations are found in the tropical eastern and central Pacific in both the pre- and post-1993 periods. However, there are noticeable differences between these two periods in the temporal evolution of the correlations. During the pre-1993 period (Fig. 3c), negative SST correlations appear near the South American coast in fall, extend westward to the tropical central Pacific in winter, and develop and peak in the central-to-eastern Pacific in the following spring and summer. These SST correlations resemble the spatial structure and temporal evolution of SST anomalies during the EP ENSO described in Kao and Yu (2009). During the post-1993 period (Fig. 3d), negative SST correlations appear off Baja California in fall, spread toward the equatorial central Pacific in winter, and grow and peak in the central-to-eastern Pacific in spring and summer. This SST correlation pattern resembles the evolution of SST anomalies during the CP ENSO. Figure 3 indicates that the SAM is correlated only with the CP ENSO, whereas the PSA is correlated with both the EP ENSO and the CP ENSO. The more frequently occurring CP ENSO after the early 1990s excites both the PSA and SAM to give rise to the in-phase PSA–SAM correlation during the most recent two decades. Based on this result, we hypothesize that the change of ENSO from the EP type to the CP type caused the early 1990s change in the ENSO–PSA–SAM relationships.

4. Composite analyses with the two types of ENSO

To further confirm our hypothesis, we form composites of the tropical Pacific SST and SH circulation anomalies for the two types of ENSO. Yu et al. (2012b) classified the major El Niño events since 1950 into the CP and EP types. Our analysis period includes 13 CP El Niño events (1953/54, 1957/58, 1958/59, 1963/64, 1965/66, 1968/69, 1977/78, 1987/88, 1991/92, 1994/95, 2002/03, 2004/05, and 2009/10) and 8 EP El Niño events (1951/52, 1969/70, 1972/73, 1976/77, 1982/83, 1986/87, 1997/98, and 2006/07). Figures 4a and 4b show the spring SST anomalies composited from these two groups of El Niño events. As expected, the CP type of El Niño events (Fig. 4a) is characterized by SST anomalies mostly confined to the central Pacific near the international date line, covering the Niño-4 (5°S–5°N, 160°E–150°W) and Niño-3.4 (5°S–5°N, 170°–120°W) regions as outlined by the blue boxes. The EP type (Fig. 4b) is characterized by SST anomalies extending from the South American coast to the central Pacific, covering the Niño-1+2 (10°S–0°, 80°–90°W) and Niño-3 (5°S–5°N, 150°–90°W) regions. The EP El Niño tends to have stronger intensity (e.g., a maximum of 2.3°C in the Niño-1+2 region) than the CP El Niño (e.g., a maximum of 1.4°C in the Niño-4 region).

Figures 4c and 4d show the composite Z500 anomalies during spring for the two types of ENSO. In the CP El Niño composite (Fig. 4c), the height anomalies exhibit a zonally symmetric structure that has positive height anomalies covering Antarctica and a negative anomaly belt centered around the midlatitudes (~30°–45°S). This structure resembles more the negative phase of the SAM (cf. Fig. 1a). In the EP El Niño composite (Fig. 4d), the height anomalies are characterized by a wave train pattern in the Western Hemisphere with three anomaly centers to the east of New Zealand (35°S, 145°W), in the Amundsen–Bellingshausen Seas (62°S, 100°W), and near the southern tip of South America (47°S, 50°W).

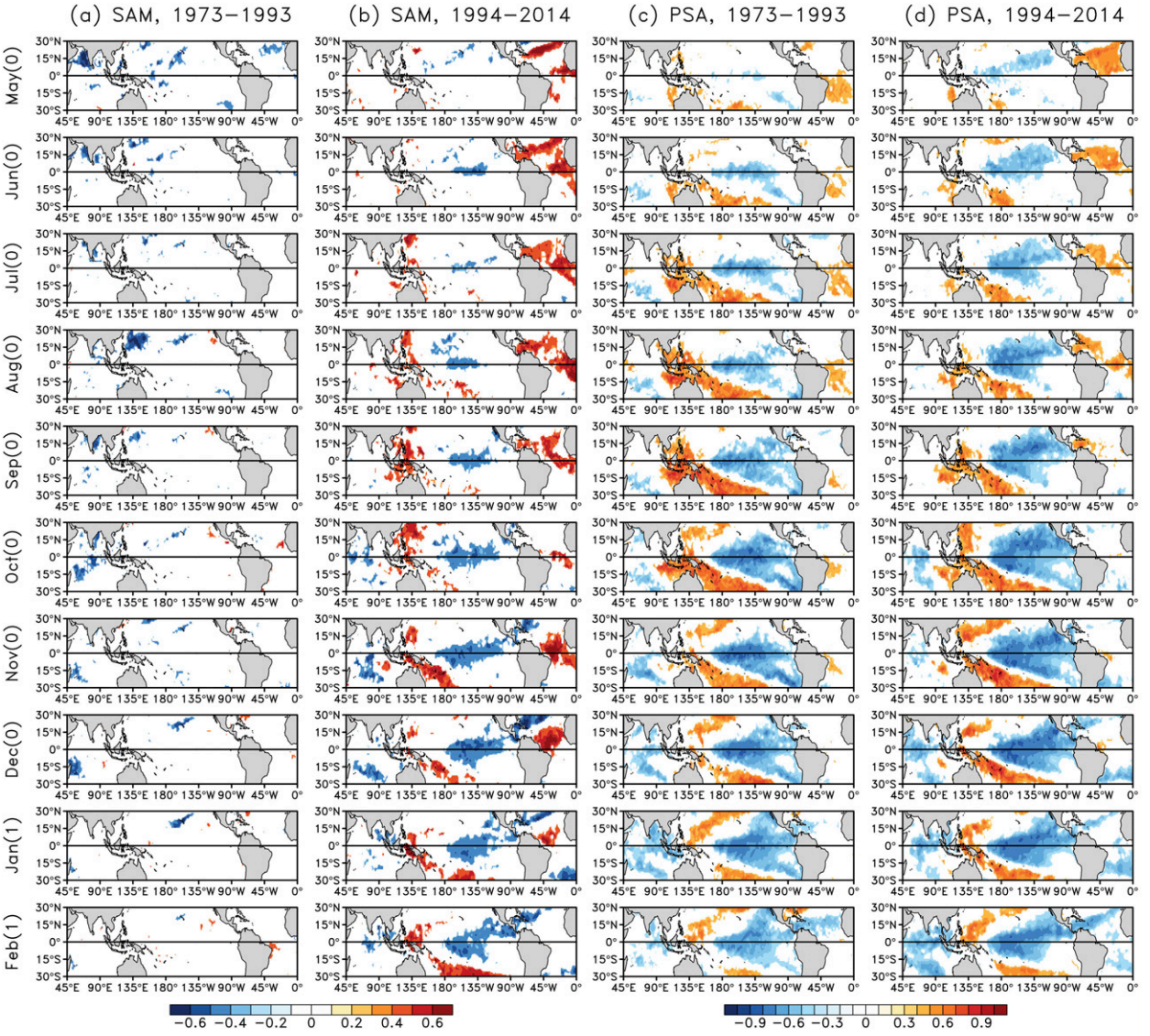

FIG. 3. Correlation coefficients between tropical SST anomalies [from (top) May to (bottom) February] and the spring (SON) SAM index for the periods of (a) 1973–93 and (b) 1994–2014. The correlations with the spring PSA index are shown for the periods (c) 1973–93 and (d) 1994–2014. Only areas with correlation coefficients at the 90% interval are shown.

This structure resembles the negative phase of the PSA (cf. Fig. 1b). Additionally, there is an anomaly center in the eastern Hemisphere between Australia and Antarctica. We also found that 9 of the 13 CP El Niño events (69%) exhibited the negative SAM in spring (1953, 1957, 1965, 1968, 1991, 1994, 2002, 2004, and 2009), while only 3 of the 8 EP El Niño events (37%) exhibited the negative SAM (1951, 1997, and 2006).

To further identify the SAM and PSA signals in the composites, we separated the composite Z500 anomalies into zonally symmetric (i.e., zonal-mean) and zonally asymmetric (i.e., zonal-mean removed) components. Figure 5a compares the zonally symmetric components from the CP and EP El Niño composites with the zonal-mean component from the negative phase of the SAM shown in Fig. 1a. The negative SAM (black line) shows a meridional dipole structure with a positive height anomaly centered at high latitudes (~75°S) and a negative height anomaly centered at midlatitudes (~45°S). The CP El Niño composite (blue line) exhibits a dipole structure with the centers located at similar latitudes of the SAM. Although the EP El Niño composite (red line) also exhibits a dipolar structure, its two anomaly centers do not match those of the SAM. In addition, the zonally symmetric component is stronger in the CP El Niño composite than in the EP El Niño composite, despite the

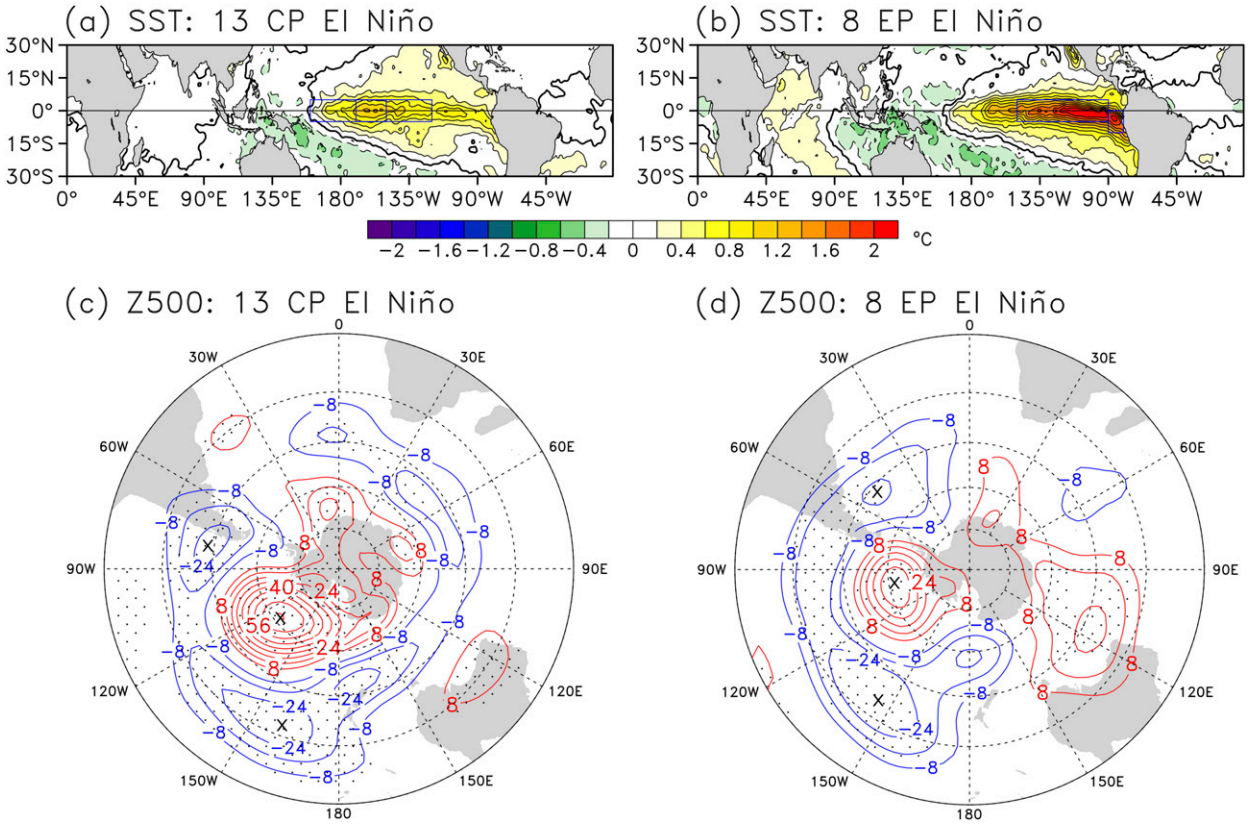

FIG. 4. (a),(b) Composite SST anomalies and (c),(d) Z500 anomalies in SON for the (left) CP El Niño and (right) EP El Niño. Dots indicate regions where the composite anomalies exceed the 95% confidence interval using a two-tailed Student's *t* test. Boxes in (a),(b) indicate the Niño-4, Niño-3.4, Niño-3, and Niño-1+2 regions. Crosses in (c),(d) indicate the local maxima and minima of the anomaly centers. Contour intervals are 8 m for (c) and (d).

fact that the EP El Niño is typically stronger than the CP El Niño in terms of their tropical Pacific SST anomalies (see Figs. 4a and 4b). As for the zonally asymmetric components, although the CP El Niño composite shows a strong zonally symmetric structure (see Fig. 4c), its zonally asymmetric component is similar to the PSA pattern (Fig. 5b). The EP El Niño composite (Fig. 5c) exhibits an anomaly pattern in the South Pacific and Atlantic sectors similar to the PSA anomaly pattern shown in Fig. 4d. Figures 4 and 5 together confirm that

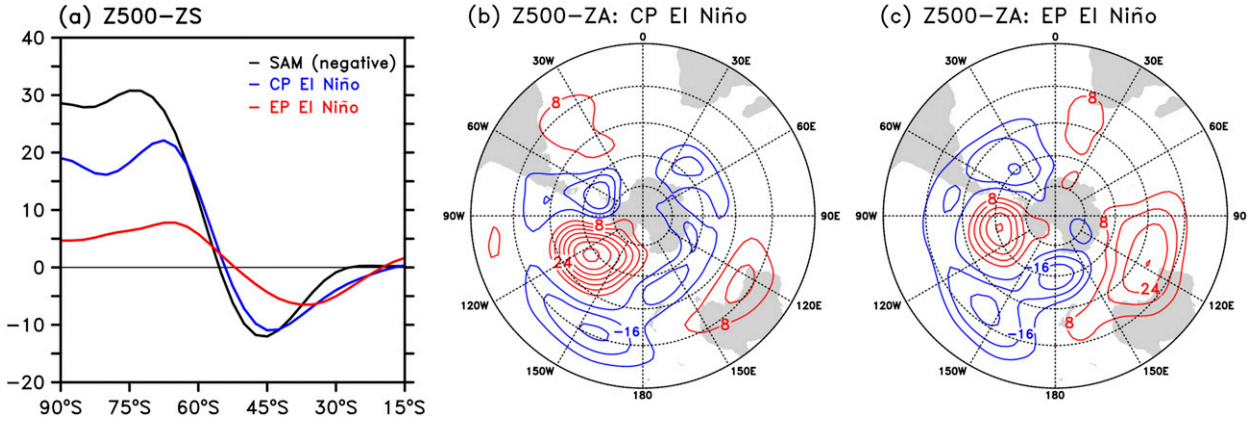

FIG. 5. (a) The zonally symmetric components of the composite Z500 anomalies (m) from the CP El Niño composite (blue line) and the EP El Niño composite (red line) compared with the zonal-mean profile of the negative phase of the SAM (black line). The zonally asymmetric components are from (b) the CP El Niño composite and (c) the EP El Niño composite. Contour intervals are 8 m in (b),(c).

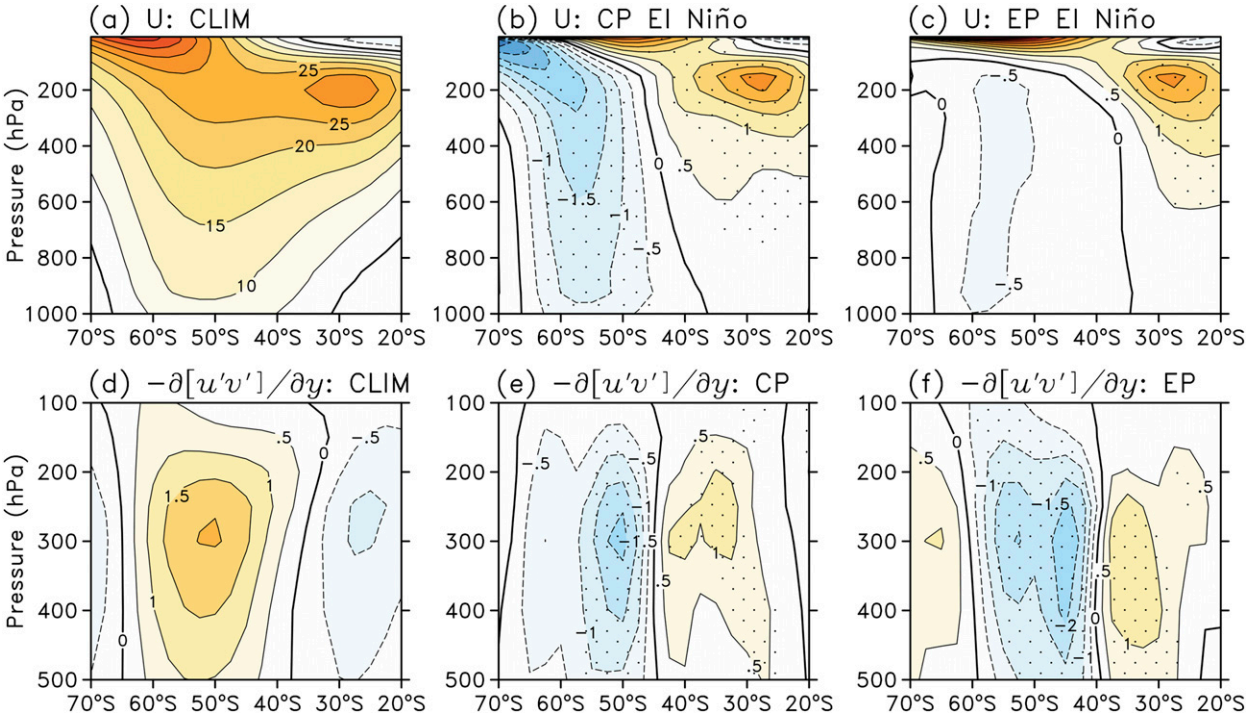

FIG. 6. Vertical structures of the climatological zonal-mean (a) zonal wind and (d) transient eddy momentum flux convergence. The zonal wind anomalies are for (b) the CP El Niño composite and (c) the EP El Niño composite, and (e),(f) their anomalous transient eddy momentum flux convergences, respectively. Contour intervals are 5 m s^{-1} in (a); 0.5 m s^{-1} in (b),(c); 0.5 × 10^{-5} m s^{-2} in (d); and 0.5 × 10^{-6} m s^{-2} in (e),(f). Values exceeding the 95% confidence interval determined using a two-tailed Student's t test are dotted.

the CP ENSO can induce both the SAM and PSA, while the EP ENSO can induce only the PSA.

5. Mechanisms linking the two types of ENSO to SAM

Why does the CP ENSO induce the SAM while the EP ENSO does not? Two mechanisms have been suggested in previous studies to link ENSO to the SAM: an eddy–mean flow interaction mechanism in the troposphere and a stratospheric pathway mechanism. The eddy–mean flow interaction mechanism requires that, during El Niño events, the increased meridional temperature gradient associated with a tropical tropospheric warming (Chiang and Sobel 2002) produce a strengthened and equatorward-displaced subtropical jet. The strengthened subtropical jet then affects the propagation of transient eddies to change the location of eddy momentum flux convergence. The changed eddy momentum flux convergence then accelerates westerly anomalies on the equatorward side of the midlatitude jet and accelerates easterly anomalies on the poleward side to give rise to a negative phase of the SAM (e.g., Seager et al. 2003). To examine these processes, we show the vertical structures of the climatology of the zonal-mean zonal wind in SON (Fig. 6a) and the corresponding anomalies composited for the CP and EP El Niño events (Figs. 6b and 6c). Both composites show significant westerly anomalies over the subtropical regions (i.e., 20°–30°S), which reflect a strengthened and equatorward-displaced subtropical jet (centered at 30°S; see Fig. 6a). However, over middle-to-high latitudes (i.e., 30°–70°S), these two composites are very different. While the EP El Niño composite (Fig. 6c) shows weak and nonsignificant variations, the CP El Niño composite (Fig. 6b) produces a negative phase–like SAM response that is characterized by positive wind anomalies (over 30°–45°S) equatorward of the midlatitude jet (centered at 50°S; see Fig. 6a) and negative wind anomalies (over 50°–70°S) poleward of the jet. The midlatitude jet is known to be eddy driven, with a central location that coincides with the center of the climatological transient eddy momentum flux convergence (shown in Fig. 6d). We then examine the anomalous transient eddy momentum flux convergence to see if the eddy–mean flow interaction mechanism is at work. Both the CP El Niño (Fig. 6e) and EP El Niño (Fig. 6f) composites produce a band of strong westerly momentum flux convergence around 30°–45°S and a band of strong easterly momentum flux convergence around 45°–60°S. The locations of these momentum flux convergence bands

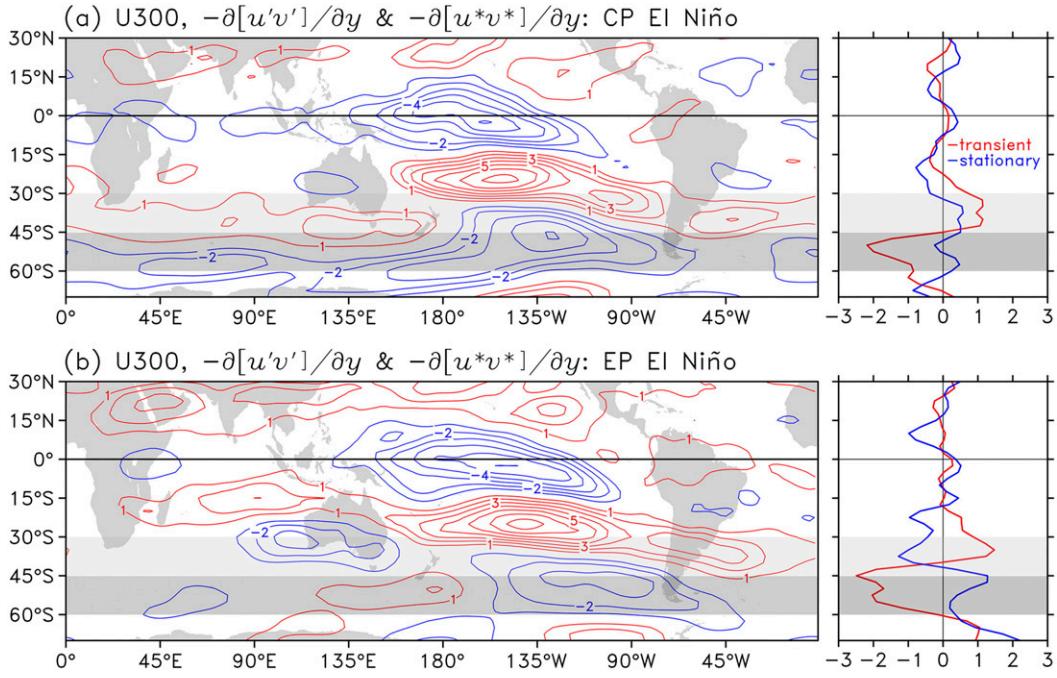

FIG. 7. (left) Composite 300-hPa zonal wind anomalies and (right) transient eddy momentum flux convergence (red lines) and stationary eddy momentum flux convergence (blue lines) for the (a) CP El Niño and (b) EP El Niño events. Contour intervals are 1 m s^{-1} for the left panels and the units are 10^{-6} m s^{-2} for the right panels. Light (dark) gray shading indicates the equatorward (poleward) side of the midlatitude jet.

coincide with the locations of the westerly and easterly wind anomaly bands for the CP El Niño (Fig. 6b) but not for the EP El Niño (Fig. 6c). The results of this analysis indicate that the transient eddy momentum flux convergence and the associated eddy–mean flow interaction can induce the SAM pattern during the CP ENSO but not during the EP ENSO.

To understand why the transient eddy momentum flux convergence cannot induce the SAM for the EP ENSO, we examine the 300-hPa zonal wind in Fig. 7. From this figure (left panels), we notice that the CP El Niño and EP El Niño composites are similar in producing a stationary wave train emanating from the tropical Pacific that represents the PSA. However, the two composites differ over the Indian Ocean sector, where a stationary wave train pattern emanating from the tropics can be found in the EP El Niño composite but not in the CP El Niño composite. This wave train pattern is associated with the Indian Ocean SST anomalies induced by the EP El Niño (see Fig. 4b), which are characterized by an east–west SST anomaly dipole resembling the Indian Ocean dipole (IOD; Saji et al. 1999; Webster et al. 1999). The IOD is known to peak in SON and be capable of exciting a wave train that propagates toward high latitudes (Lau and Nath 2004; Yu and Lau 2005; Cai et al. 2011). We also analyze the momentum flux convergence of the stationary waves in the EP El Niño composite and display its zonal-mean values in Fig. 7b (right panel). It is interesting to note the zonal means (blue line) tend to be of opposite sign to those of the momentum flux convergence produced by transient eddies (red line). As a result of this cancellation, the eddy–mean flow interaction mechanism is not able to produce a SAM pattern during EP El Niño events. In contrast, during the CP El Niño (Fig. 7a), the zonal means of the stationary eddy momentum flux convergence are relatively weak compared to the transient eddy momentum flux convergence. The anomalous transient eddy momentum flux associated with the CP El Niño produces positive and negative wind anomalies, respectively, on the equatorward (shaded in light gray) and poleward (shaded in dark gray) sides of the midlatitude jet over most of the SH, except over the Pacific, to give rise to a SAM pattern. Figure 7 indicates that the different influences of the two types of ENSO on the Indian Ocean SST anomalies enable these two ENSO types to produce difference influences on the SAM through eddy–mean flow interactions. It is noted that the value of the stationary eddy momentum flux convergence is weakly positive at the equator in our Fig. 7 (right panels), which is different from the weakly negative value reported in Seager et al. (2003). We were able to determine that the reason for this difference was the different analysis methods used in these two studies (not shown).

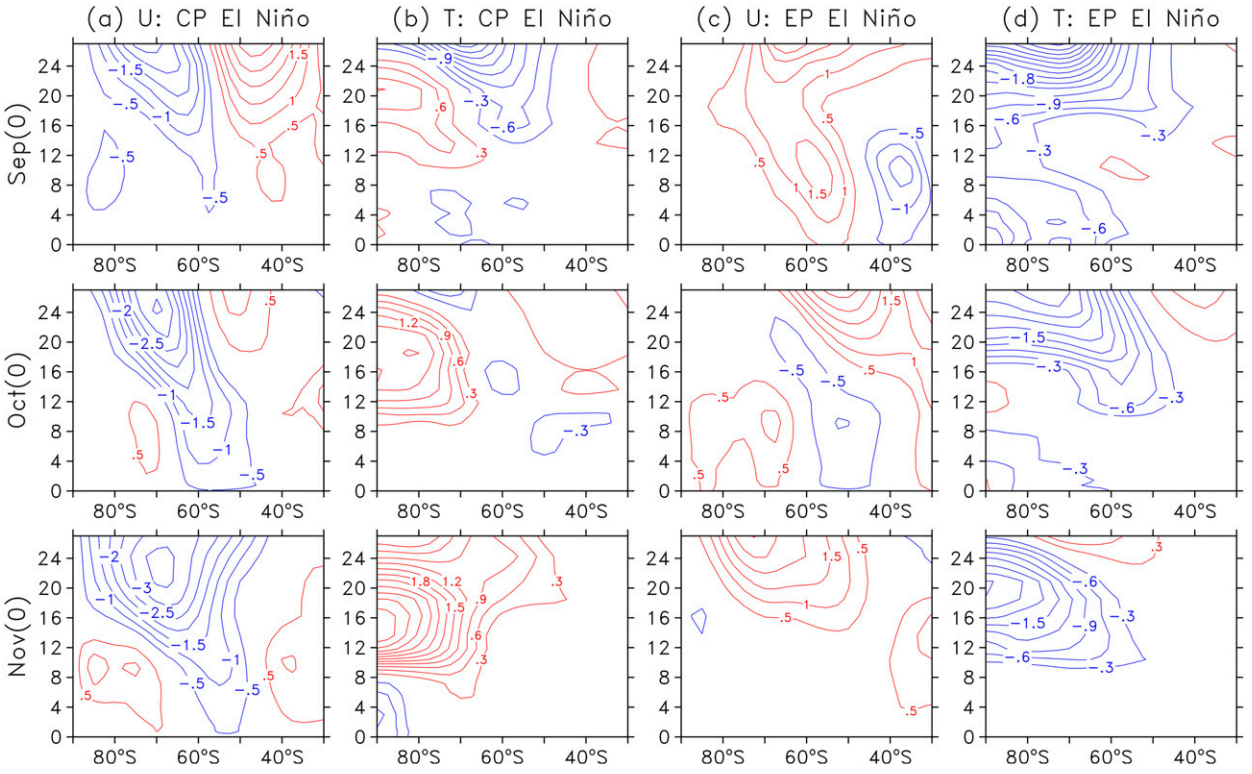

FIG. 8. Evolution of the zonal-mean zonal wind U and air temperature T anomalies from the (a),(b) CP El Niño composite and the (c),(d) EP El Niño composite during the spring season [from (top) September to (bottom) November]. The ordinate is height (km) and the abscissa is latitude. Contour intervals are 0.5 m s^{-1} for wind and 0.3°C for temperature.

We next examine the stratospheric pathway mechanism. This mechanism suggests that ENSO can induce planetary waves leading to a stratospheric polar warming (Hurwitz et al. 2011, 2013; Zubiaurre and Calvo 2012). The associated longitudinal temperature variations weaken the polar vortex, whose associated circulation anomalies can later descend into the troposphere to give rise to the SAM (Son et al. 2013; Evtushevsky et al. 2015). The evolution of the zonal wind and temperature anomalies composited for the two types of El Niño during the spring season are shown in Fig. 8. The CP El Niño composite exhibits a weakening of the polar vortex (i.e., the negative wind anomalies over the region above 16 km and poleward of 60°S; Fig. 8a) in September, which is accompanied by a stratospheric warming centered at 20 km in the polar region (Fig. 8b). The wind and temperature anomalies in the stratosphere then descend to the troposphere in the following months (October–November) to give rise to a negative phase of SAM with easterly anomalies around 60°S and westerly anomalies around 40°S (see Fig. 8a). In contrast, the EP El Niño composite does not show a weakening in the westerlies in the polar stratosphere nor a warming there (Figs. 8c and 8d). To confirm that the composite result is not overly influenced by any particular El Niño event, we repeated the analysis with the 2002 El Niño event excluded (this particular event is known to produce a massive Antarctic stratospheric sudden warming; Newman and Nash 2005) and found similar results (not shown). The analyses we presented in this section suggest that both the eddy–mean flow interaction and the stratospheric pathway mechanisms enable the CP ENSO to influence SAM variability in the SON season.

6. The changing impacts of ENSO on SH climate

In this section, we investigate how the post-1993 ENSO–PSA–SAM relationships impacted the Antarctic climate. We first examine the intensities of SAM and PSA using the 15-yr running variance of these two indices. The SAM variance increased after the early 1990s (red line in Fig. 9a), which is likely a manifestation of the additional contribution from the CP ENSO forcing to the SAM variability. The PSA variance does not show a substantial change (blue line in Fig. 9a), implying that it is not affected by the change of ENSO type in the early 1990s.

As mentioned, the SAM and PSA share a common anomaly center over the Amundsen–Bellingshausen Seas (ABS). This region is one of the best locations to detect the impact of the changing ENSO–PSA–SAM

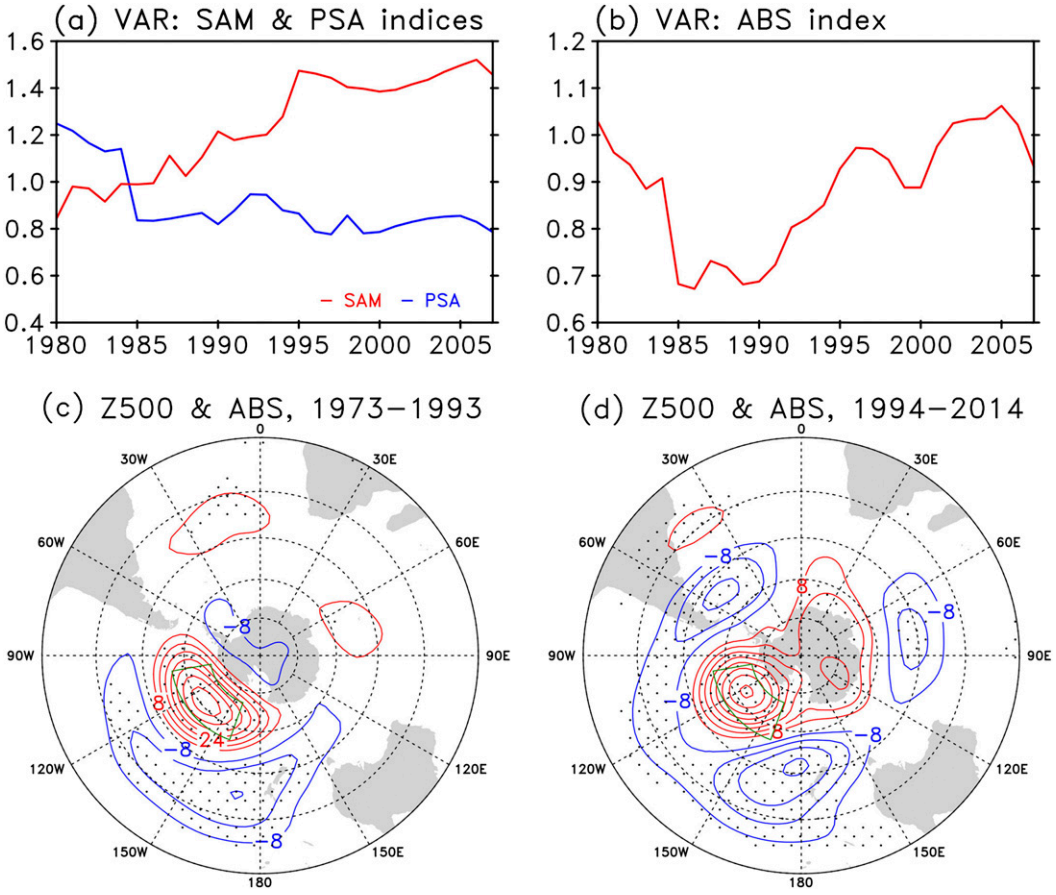

FIG. 9. (top) The 15-yr running variance for (a) the SAM (red line) and PSA (blue line) indices and (b) the standardized ABS index. (bottom) Regressed Z500 anomalies on the ABS index in SON for the periods (c) 1973–93 and (d) 1994–2014. Green boxes indicate the region where the ABS index is defined. Values exceeding the 95% confidence interval are dotted. Contour intervals are 8 m in (c),(d).

relationships (or the changing ENSO type) on the SH climate. We defined an ABS index as the Z500 anomalies averaged over 55°–75°S, 100°–140°W (Figs. 9c and 9d). A 15-yr running variance of this index indicates an increase in the ABS intensity after the early 1990s (Fig. 9b). Correlating the ABS index with the SAM and PSA indices shows that 92% of the total variance of the ABS index is explained by the SAM and PSA indices. Comparing the Z500 anomalies regressed onto the spring ABS index in the pre-1993 period and in the post-1993 period shows that the positive ABS height anomalies intensified during the post-1993 period (Figs. 9c and 9d). Therefore, the strengthened ABS height anomalies in recent decades can be explained as a result of both the intensified SAM and the increasingly in-phase relationship between the SAM and PSA.

The ABS variability has profound impacts on sea ice concentrations (SICs) in the Southern Ocean (e.g., Turner et al. 2013). Geopotential height variations over the ABS region can induce anomalous eddy heat and momentum fluxes to produce the so-called Antarctic sea ice dipole structure (ADP; Yuan and Martinson 2001), which is characterized by out-of-phase SIC anomalies between the Pacific and Atlantic sectors. We examine the variation of the spring ABS index from 1979 to 2014 and note the amplitude of the variation increased after the early 1990s (Fig. 10a, top panel). The ADP can be identified from the longitudinal distribution of the SIC anomalies over the 60°–70°S belt in early summer [November–January (NDJ)] as the out-of-phase anomalies between the Pacific sector over 130°–150°W and the Atlantic sector over 40°–60°W (Fig. 10a, bottom panel). Consistent with the increasing ABS index, the amplitude of the ADP also increased after the early 1990s. Following Yuan (2004), we compute the ADP index as the difference between the SIC anomalies averaged in a South Pacific box (60°–70°S, 130°–150°W) and an Atlantic box (60°–70°S, 40°–60°W). Yuan and Li (2008) suggested that the correlations between atmospheric circulation modes and sea ice anomalies are the strongest when the ice lags

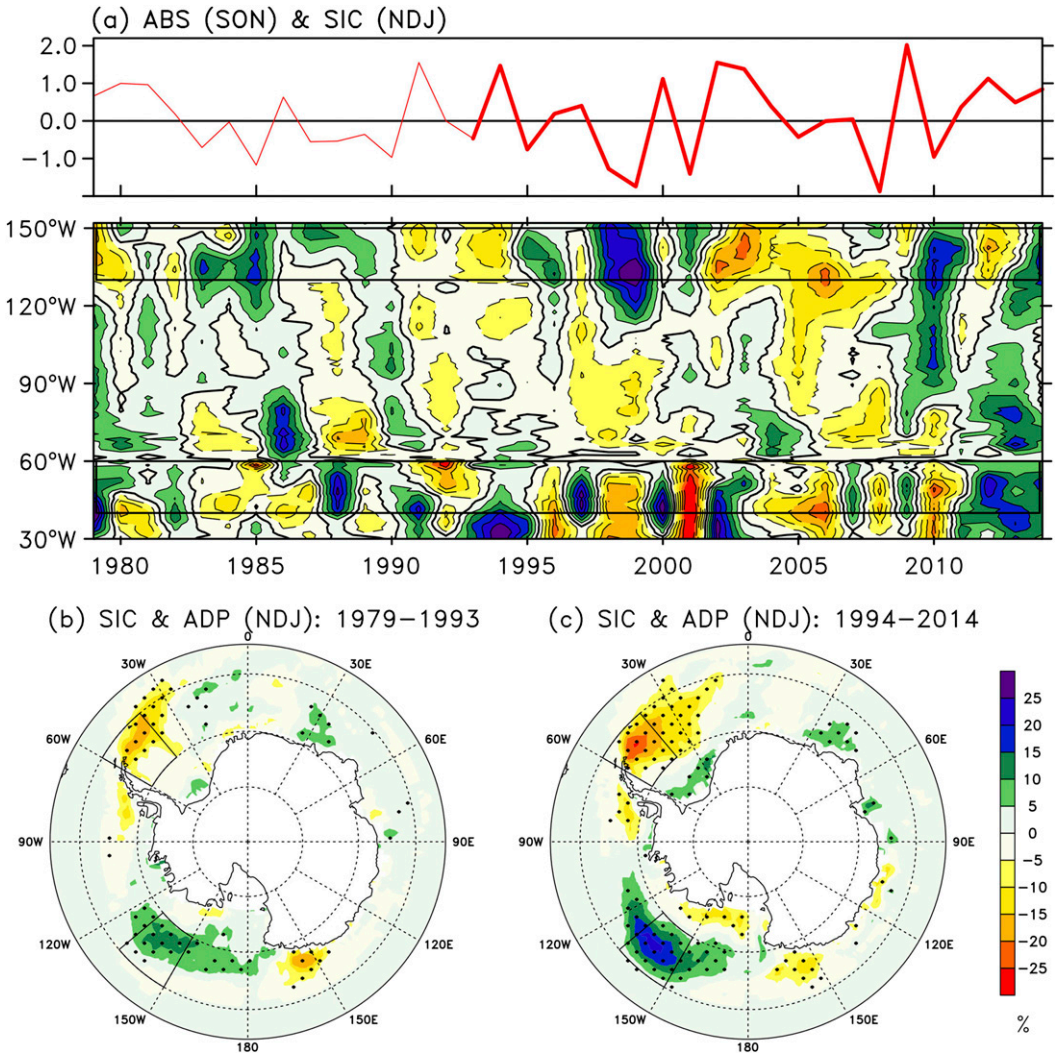

FIG. 10. (a) Time series of the standardized ABS index in SON at top and the longitudinal distribution of SIC anomalies at bottom (%) averaged over 60°–70°S in the early summer (NDJ). The thick red line emphasizes the intensified ABS after the early 1990s. Black boxes in the bottom of (a) indicate the Pacific sector (top box; 130°–150°W) and Atlantic sector (bottom box; 40°–60°W) of the ADP. Regressed SIC anomalies onto the ADP index in NDJ for the periods (b) 1979–93 and (c) 1994–2014. Black boxes in (b),(c) indicate the regions where the ADP index is defined. The areas exceeding the 95% interval determined using a two-tailed Student's *t* test are dotted.

the circulation modes by 2 months. We regressed SIC anomalies onto the ADP index in the NDJ season separately for the pre-1993 and post-1993 periods. During the pre-1993 period (1979–93; Fig. 10b), positive SIC anomalies occur in the Pacific sector over the Ross Sea and negative anomalies occur in the Atlantic sector over west of Weddell Sea. During the post-1993 period (1994–2014; Fig. 10c), the dipole structure is similar to that in the previous period. However, the ADP has stronger amplitudes in the post-1993 period than in the pre-1993 period. Our analysis indicates that the sea ice dipolar structure induced by ENSO becomes stronger after ENSO changed from the EP to the CP type in the early 1990s.

We next examined the possible impact of the changing ENSO–PSA–SAM relationships on Antarctic surface air temperatures. We applied an EOF analysis to find the leading variability modes in spring surface air temperature (SAT) anomalies over 30°–90°S. The structures of the first two leading EOF modes (EOF1 and EOF2, respectively) are shown in Figs. 11a and 11b. Both modes exhibit a dipolar structure with a temperature anomaly center over the Weddell Sea that is out of phase with an anomaly center over the Ross Sea. The two EOFs are different in that surface temperature anomalies over East Antarctica are in phase with the temperature anomaly center over the Ross Sea in EOF1 but are in phase with the anomaly

center over the Weddell Sea in the EOF2. EOF1 and EOF2 together suggest that surface air temperature variations over Antarctica are largest in three regions: East Antarctica, West Antarctica (related to the anomaly center over the Ross Sea), and the Antarctica Peninsula (related to the anomaly center over the Weddell Sea). Associated with the anomaly dipole in EOF1 and EOF2, surface temperature variations over the Antarctic Peninsula and West Antarctica tend to be out of phase when either one of the EOF modes dominates. However, surface temperature variations over East Antarctica can be in phase with those over West Antarctica when EOF1 dominates, or in phase with those over the Antarctic Peninsula when EOF2 dominates. When the amplitudes of EOF1 and EOF2 are comparable, their temperature anomalies over East Antarctica tend to cancel each other out. In that case, temperature variations in East Antarctica would be not correlated with either those in West Antarctica or those in the Antarctic Peninsula.

To examine the linkages between these two EOF modes and the SAM and PSA, we regressed surface air temperature anomalies onto the inverted SAM and PSA indices. It is interesting that the SAM regression pattern resembles EOF1 whereas the PSA regression pattern resembles EOF2 (Figs. 11c and 11d). The correlation coefficient between the SAM index and principal component of EOF1 is −0.79, indicating that EOF1 is more associated with the SAM. The correlation coefficient between the PSA and principal component of EOF2 is −0.47, indicating that EOF2 is more associated with the PSA. Based on these linkages, we expect the EP El Niño influence on Antarctic surface air temperature to be close to that of EOF2 because the EP El Niño can excite a negative phase of PSA. Figure 11f shows the surface air temperature anomalies composited from the EP El Niño events. As expected, the EP El Niño composite is similar to EOF2, with the temperature anomalies over the Antarctic Peninsula out of phase with the anomalies over West Antarctica and in phase with the anomalies over East Antarctica. The CP El Niño composite for surface temperature anomalies is shown in Fig. 11e. In this composite, significant temperature anomalies over the Antarctica are found only over West Antarctica and the Antarctic Peninsula, with their anomalies out of phase. Temperature anomalies over East Antarctica are weak and are mostly not statistically significant. These two features can be explained by our finding that the CP El Niño can excite both a negative phase of PSA and a negative phase of SAM. As a result, the CP El Niño composite should resemble the combined pattern of EOF1 and EOF2, which tends to cancel out surface temperature anomalies over East Antarctica and at the same time intensify the out-of-phase relationships between the temperature anomalies over the Antarctic Peninsula and West Antarctica.

7. Conclusions

In this study, we examined the decadal variations in the relationships among ENSO, the SAM, and the PSA to understand how the ENSO influence on the high-latitude Southern Hemisphere has varied during the past seven decades. It is our conclusion that the change in ENSO type in the early 1990s altered the mechanisms and spatial patterns of ENSO influence on Southern Hemisphere climate. Before the early 1990s, ENSO was dominated by the EP type, which influenced the Southern Hemisphere climate via an excitation of the PSA wave train pattern. The ENSO–Southern Hemisphere influence was strong in some events but weak in others, depending on the random phase relationship between the PSA and the internally generated SAM. After the early 1990s, the dominant CP ENSO modulated not only the PSA but also the SAM. As a result, the SAM and PSA events became more in phase after the early 1990s. The increasing influence of the CP ENSO on the SAM is accomplished through both an eddy–mean flow interaction mechanism and a stratospheric pathway mechanism.

The changing ENSO–PSA–SAM relationships have rendered ENSO more effective in influencing the Southern Hemisphere after the early 1990s. Two such impacts were identified in this study. One of them is related to the sea ice dipole pattern around the Antarctic Peninsula, and the other is related to the phase correlations of the surface air temperature variations in East Antarctica, West Antarctica, and the Antarctic Peninsula. While the sea ice dipole has been known to be related to the ENSO forcing (Yuan 2004), we find the dipole to be stronger after ENSO changed to the CP type. The in-phase relationship between the PSA and SAM enhanced the geopotential height anomalies over the Amundsen–Bellingshausen Seas. The different ENSO types also have different footprints on Antarctic surface air temperature patterns. The EP ENSO tends to link surface temperature variations across the entire Antarctic continent, while the CP ENSO tends to link the temperature variations between West Antarctica and the Antarctic Peninsula only.

The findings in this study can help explain the changing role of ENSO in decadal and interannual variability in high-latitude Southern Hemisphere climate. Such changes have implications for sea ice, ocean circulation, biogeochemistry, and ecology. The relationships found here among ENSO, SAM, and PSA could potentially be used in conjunction with Antarctic paleo-temperature records to examine changes in ENSO type on longer time scales. This study does not examine the reasons why the early 1990s change in the PSA–SAM relationship is observed only during the SON season. Pursuit of this question will

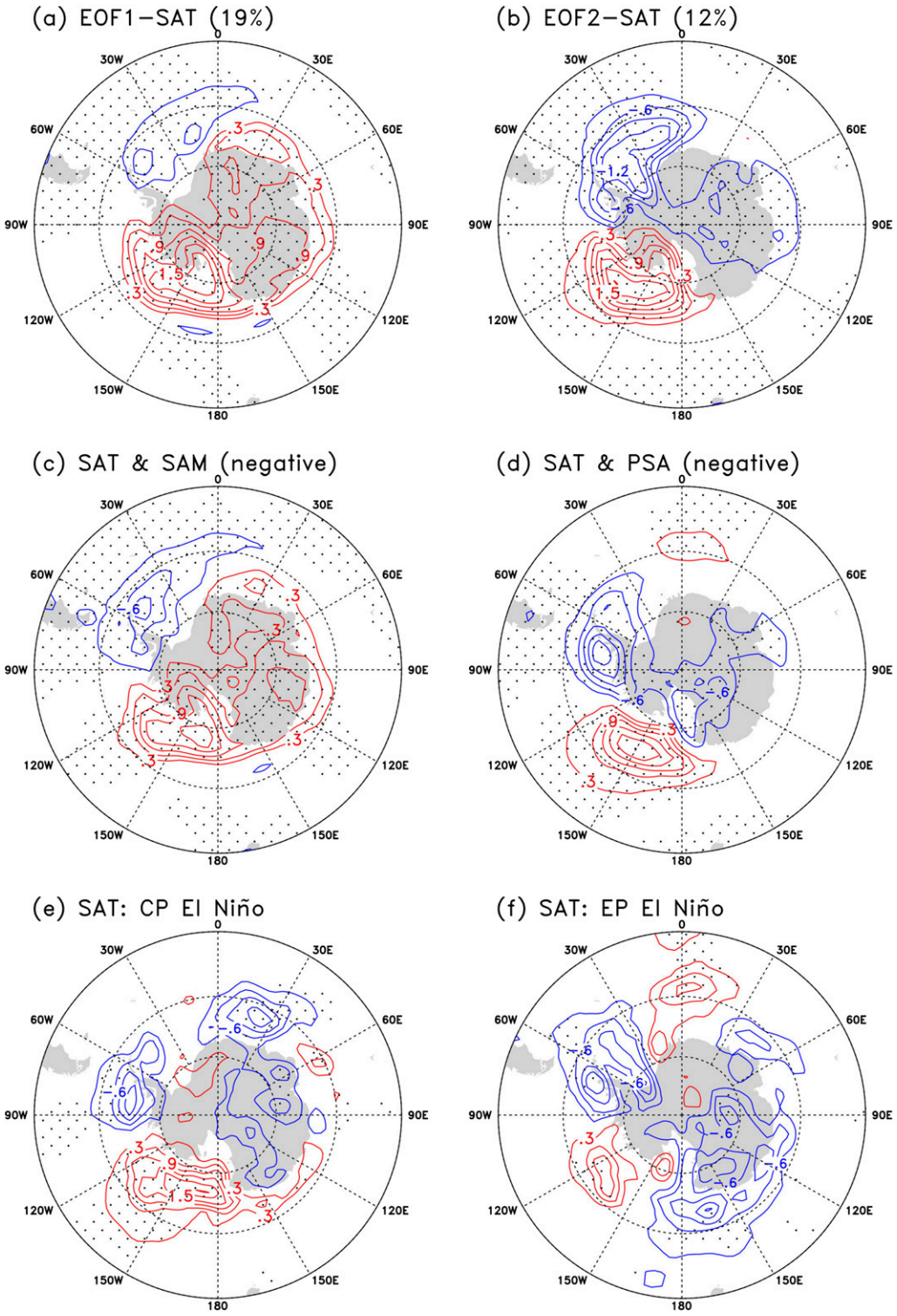

FIG. 11. (top) Spatial structures of the (a) first EOF mode and (b) second EOF mode of the SAT anomalies in SON. (middle) Regressed surface temperature anomalies onto the inverted (c) SAM index and (d) PSA index. (bottom) Surface temperature anomalies for (e) the CP El Niño composite and (f) the EP El Niño composite. Contour intervals are 0.3°C. Values exceeding the 95% interval determined using a two-tailed Student's t test are dotted.

require further analysis of the other three seasons and is beyond the scope of this study. Nevertheless, it is possibly related to the seasonal differences in the SH atmospheric circulation, such as the strength and location of the subtropical and eddy-driven jet streams, which support different wave train and transient eddy responses. It should also be noted that this study is an empirical study and that modeling studies are needed to reach more definite conclusions on the causality of the early 1990s change.

Acknowledgments. The authors thank two anonymous reviewers and Editor John Walsh for their very constructive comments that have helped improve the paper. This research was supported by NSF's Climate and Large-scale Dynamics Program under Grants AGS-1233542 and AGS-1505145. The effort by Tong Lee was carried out at the Jet Propulsion Laboratory, California Institute of Technology, under a contract with the National Aeronautics and Space Administration. The NCEP–NCAR reanalysis data were obtained at www.esrl.noaa.gov/psd, HadISST data are available at www.metoffice.gov.uk/hadobs/hadisst, and the SAM* index data are available at http://www.nerc-bas.ac.uk/icd/gjma/sam.html.

REFERENCES

Bromwich, D. H., J. P. Nicolas, A. J. Monaghan, M. A. Lazzara, L. M. Keller, G. A. Weidner, and A. B. Wilson, 2013: Central West Antarctica among the most rapidly warming regions on Earth. *Nat. Geosci.*, **6**, 139–145, doi:10.1038/ngeo1671.

Cai, W., P. V. Rensch, T. Cowan, and H. H. Hendon, 2011: Teleconnection pathways for ENSO and the IOD and the mechanisms for impacts on Australian rainfall. *J. Climate*, **24**, 3910–3923, doi:10.1175/2011JCLI4129.1.

Chiang, J. C. H., and A. H. Sobel, 2002: Tropical tropospheric temperature variations caused by ENSO and their influence on the remote tropical climate. *J. Climate*, **15**, 2616–2631, doi:10.1175/1520-0442(2002)015<2616:TTTVCB>2.0.CO;2.

Ciasto, L. M., and D. W. J. Thompson, 2008: Observations of large-scale ocean–atmosphere interaction in the Southern Hemisphere. *J. Climate*, **21**, 1244–1259, doi:10.1175/2007JCLI1809.1.

——, G. R. Simpkins, and M. H. England, 2015: Teleconnections between tropical Pacific SST anomalies and extratropical Southern Hemisphere climate. *J. Climate*, **28**, 56–65, doi:10.1175/JCLI-D-14-00438.1.

Codron, F., 2005: Relation between annular modes and the mean state: Southern Hemisphere summer. *J. Climate*, **18**, 320–330, doi:10.1175/JCLI-3255.1.

Ding, Q., E. J. Steig, D. S. Battisti, and M. Kuettel, 2011: Winter warming in West Antarctica caused by central tropical Pacific warming. *Nat. Geosci.*, **4**, 398–403, doi:10.1038/ngeo1129.

Evtushevsky, O. M., V. O. Kravchenko, L. L. Hood, and G. P. Milinevsky, 2015: Teleconnection between the central tropical Pacific and the Antarctic stratosphere: Spatial patterns and time lags. *Climate Dyn.*, **44**, 1841–1855, doi:10.1007/s00382-014-2375-2.

Feldstein, S. B., and S. Lee, 1998: Is the atmospheric zonal index driven by an eddy feedback? *J. Atmos. Sci.*, **55**, 3077–3086, doi:10.1175/1520-0469(1998)055<3077:ITAZID>2.0.CO;2.

Fogt, R. L., and D. H. Bromwich, 2006: Decadal variability of the ENSO teleconnection to the high-latitude South Pacific governed by coupling with the southern annular mode. *J. Climate*, **19**, 979–997, doi:10.1175/JCLI3671.1.

Hartmann, D. L., and F. Lo, 1998: Wave-driven zonal flow vacillation in the Southern Hemisphere. *J. Atmos. Sci.*, **55**, 1303–1315, doi:10.1175/1520-0469(1998)055<1303:WDZFVI>2.0.CO;2.

Hurwitz, M. M., P. A. Newman, L. D. Oman, and A. M. Molod, 2011: Response of the Antarctic stratosphere to two types of El Niño events. *J. Atmos. Sci.*, **68**, 812–822, doi:10.1175/2011JAS3606.1.

——, C. I. Garfinkel, P. A. Newman, and L. D. Oman, 2013: Sensitivity of the atmospheric response to warm pool El Niño events to modeled SSTs and future climate forcings. *J. Geophys. Res. Atmos.*, **118**, 13 371–13 382, doi:10.1002/2013JD021051.

Jin, D., and B. P. Kirtman, 2009: Why the Southern Hemisphere ENSO responses lead ENSO. *J. Geophys. Res.*, **114**, D23101, doi:10.1029/2009JD012657.

Kalnay, E., and Coauthors, 1996: The NCEP/NCAR 40-Year Reanalysis Project. *Bull. Amer. Meteor. Soc.*, **77**, 437–471, doi:10.1175/1520-0477(1996)077<0437:TNYRP>2.0.CO;2.

Kao, H. Y., and J.-Y. Yu, 2009: Contrasting eastern Pacific and central Pacific types of El Niño. *J. Climate*, **22**, 615–632, doi:10.1175/2008JCLI2309.1.

Karoly, D. J., 1989: Southern Hemisphere circulation features associated with El Niño–Southern Oscillation events. *J. Climate*, **2**, 1239–1252, doi:10.1175/1520-0442(1989)002<1239:SHCFAW>2.0.CO;2.

Kwok, R., and J. C. Comiso, 2002: Spatial patterns of variability in Antarctic surface temperature: Connections to the South Hemisphere annular mode and the Southern Oscillation. *Geophys. Res. Lett.*, **29**, 1705, doi:10.1029/2002GL015415.

Lau, N. C., and M. J. Nath, 2004: Coupled GCM simulation of atmosphere–ocean variability associated with zonally asymmetric SST changes in the tropical Indian Ocean. *J. Climate*, **17**, 245–265, doi:10.1175/1520-0442(2004)017<0245:CGSOAV>2.0.CO;2.

Lee, T., and M. J. McPhaden, 2010: Increasing intensity of El Niño in the central-equatorial Pacific. *Geophys. Res. Lett.*, **37**, L14603, doi:10.1029/2010GL044007.

——, and Coauthors, 2010: Record warming in the South Pacific and western Antarctica associated with the strong central-Pacific El Niño in 2009–10. *Geophys. Res. Lett.*, **37**, L19704, doi:10.1029/2010GL044865.

L'Heureux, M. L., and D. W. J. Thompson, 2006: Observed relationships between the El Niño–Southern Oscillation and the extratropical zonal-mean circulation. *J. Climate*, **19**, 276–287, doi:10.1175/JCLI3617.1.

Lim, E. P., H. H. Hendon, and H. Rashid, 2013: Seasonal predictability of the southern annular mode due to its association with ENSO. *J. Climate*, **26**, 8037–8054, doi:10.1175/JCLI-D-13-00006.1.

Limpasuvan, V., and D. L. Hartmann, 2000: Wave-maintained annular modes of climate variability. *J. Climate*, **13**, 4414–4429, doi:10.1175/1520-0442(2000)013<4414:WMAMOC>2.0.CO;2.

Liu, J., J. A. Curry, and D. G. Martinson, 2004: Interpretation of recent Antarctic sea ice variability. *Geophys. Res. Lett.*, **31**, L02205, doi:10.1029/2003GL018732.

Lorenz, D. J., and D. L. Hartmann, 2001: Eddy–zonal flow feedback in the Southern Hemisphere. *J. Atmos. Sci.*, **58**, 3312–3327, doi:10.1175/1520-0469(2001)058<3312:EZFFIT>2.0.CO;2.

Marshall, G. J., 2003: Trends in the southern annular mode from observations and reanalyses. *J. Climate*, **16**, 4134–4143, doi:10.1175/1520-0442(2003)016<4134:TITSAM>2.0.CO;2.

Mechoso, C. R., D. L. Hartmann, and J. D. Farrara, 1985: Climatology and interannual variability of wave, mean–flow interaction in the Southern Hemisphere. *J. Atmos. Sci.*, **42**, 2189–2206, doi:10.1175/1520-0469(1985)042<2189:CAIVOW>2.0.CO;2.

Mo, K. C., 2000: Relationships between interdecadal variability in the Southern Hemisphere and sea surface temperature anomalies. *J. Climate*, **13**, 3599–3610, doi:10.1175/1520-0442(2000)013<3599:RBLFVI>2.0.CO;2.

——, and M. Ghil, 1987: Statistics and dynamics of persistent anomalies. *J. Atmos. Sci.*, **44**, 877–902, doi:10.1175/1520-0469(1987)044<0877:SADOPA>2.0.CO;2.

——, and R. W. Higgins, 1998: The Pacific–South American modes and tropical convection during the Southern Hemisphere winter. *Mon. Wea. Rev.*, **126**, 1581–1598, doi:10.1175/1520-0493(1998)126<1581:TPSAMA>2.0.CO;2.

——, and J. N. Paegle, 2001: The Pacific–South American modes and their downstream effects. *Int. J. Climatol.*, **21**, 1211–1229, doi:10.1002/joc.685.

Newman, P., and E. R. Nash, 2005: The unusual Southern Hemisphere stratosphere winter of 2002. *J. Atmos. Sci.*, **62**, 614–628, doi:10.1175/JAS-3323.1.

Rasmusson, E. M., and T. H. Carpenter, 1982: Variations in tropical sea surface temperature and surface wind fields associated with the Southern Oscillation/El Niño. *Mon. Wea. Rev.*, **110**, 354–384, doi:10.1175/1520-0493(1982)110<0354:VITSST>2.0.CO;2.

Rayner, N. A., D. E. Parker, E. B. Horton, C. K. Folland, L. V. Alexander, D. P. Rowell, E. C. Kent, and A. Kaplan, 2003: Global analyses of sea surface temperature, sea ice, and night marine air temperature since the late nineteenth century. *J. Geophys. Res.*, **108**, 4407, doi:10.1029/2002JD002670.

Robertson, A. W., and C. R. Mechoso, 2003: Circulation regimes and low-frequency oscillations in the South Pacific sector. *Mon. Wea. Rev.*, **131**, 1566–1576, doi:10.1175//2548.1.

Saji, N. H., B. N. Goswami, P. N. Vinayachandran, and T. Yamagata, 1999: A dipole mode in the tropical Indian Ocean. *Nature*, **401**, 360–363.

Schneider, D. P., C. Deser, and Y. Okumura, 2012: An assessment and interpretation of the observed warming of West Antarctica in the austral spring. *Climate Dyn.*, **38**, 323–347, doi:10.1007/s00382-010-0985-x.

Seager, R., N. Harnik, Y. Kushnir, W. Robinson, and J. Miller, 2003: Mechanisms of hemispherically symmetric climate variability. *J. Climate*, **16**, 2960–2978, doi:10.1175/1520-0442(2003)016<2960:MOHSCV>2.0.CO;2.

Silvestri, G. E., and C. S. Vera, 2003: Antarctic Oscillation signal on precipitation anomalies over southeastern South America. *Geophys. Res. Lett.*, **30**, 2155, doi:10.1029/2003GL018277.

Son, S.-W., A. Purich, H. H. Hendon, B. M. Kim, and L. M. Polvani, 2013: Improved seasonal forecast using ozone hole variability? *Geophys. Res. Lett.*, **40**, 6231–6235, doi:10.1002/2013GL057731.

Song, H.-J., E. Choi, G.-H. Lim, Y. H. Kim, J.-S. Kug, and S.-W. Yeh, 2011: The central Pacific as the export region of the El Niño–Southern Oscillation sea surface temperature anomaly to Antarctic sea ice. *J. Geophys. Res.*, **116**, D21113, doi:10.1029/2011JD015645.

Stammerjohn, S. E., D. G. Martinson, R. C. Smith, X. Yuan, and D. Rind, 2008: Trends in Antarctic annual sea ice retreat and advance and their relation to El Niño–Southern Oscillation and Southern Annular Mode variability. *J. Geophys. Res.*, **113**, C03S90, doi:10.1029/2007JC004269.

Sun, D., F. Xue, and T. Zhou, 2013: Impact of two types of El Niño on atmospheric circulation in the Southern Hemisphere. *Adv. Atmos. Sci.*, **30**, 1732–1742, doi:10.1007/s00376-013-2287-9.

Thompson, D. W. J., and J. M. Wallace, 2000: Annular modes in the extratropical circulation. Part I: Month-to-month variability. *J. Climate*, **13**, 1000–1016, doi:10.1175/1520-0442(2000)013<1000:AMITEC>2.0.CO;2.

Turner, J., T. Phillips, J. S. Hosking, G. J. Marshall, and A. Orr, 2013: The Amundsen Sea low. *Int. J. Climatol.*, **33**, 1818–1829, doi:10.1002/joc.3558.

Webster, P. J., A. M. Moore, J. P. Loschnigg, and R. R. Leben, 1999: Coupled ocean-atmosphere dynamics in the Indian Ocean during 1997–98. *Nature*, **401**, 356–360, doi:10.1038/43848.

Wilson, A. B., D. H. Bromwich, K. M. Hines, and S. H. Wang, 2014: El Niño flavors and their simulated impacts on atmospheric circulation in the high southern latitudes. *J. Climate*, **27**, 8934–8955, doi:10.1175/JCLI-D-14-00296.1.

Yeo, S.-R., and K.-Y. Kim, 2015: Decadal changes in the Southern Hemisphere sea surface temperature in association with El Niño–Southern Oscillation and Southern Annular Mode. *Climate Dyn.*, 1–16, doi:10.1007/s00382-015-2535-z, in press.

Yu, J.-Y., and D. L. Hartmann, 1993: Zonal flow vacillation and eddy forcing in a simple GCM of the atmosphere. *J. Atmos. Sci.*, **50**, 3244–3259, doi:10.1175/1520-0469(1993)050<3244:ZFVAEF>2.0.CO;2.

——, and K. M. Lau, 2005: Contrasting Indian Ocean SST variability with and without ENSO influence: A coupled atmosphere-ocean GCM study. *Meteor. Atmos. Phys.*, **90**, 179–191, doi:10.1007/s00703-004-0094-7.

——, and H. Y. Kao, 2007: Decadal changes of ENSO persistence barrier in SST and ocean heat content indices: 1958–2001. *J. Geophys. Res.*, **112**, D13106, doi:10.1029/2006JD007654.

——, M.-M. Lu, and S.-T. Kim, 2012a: A change in the relationship between tropical central Pacific SST variability and the extratropical atmosphere around 1990. *Environ. Res. Lett.*, **7**, 034025, doi:10.1088/1748-9326/7/3/034025.

——, Y. Zou, S.-T. Kim, and T. Lee, 2012b: The changing impact of El Niño on US winter temperatures. *Geophys. Res. Lett.*, **39**, L15702, doi:10.1029/2012GL052483.

——, P.-K. Kao, H. Paek, H.-H. Hsu, C.-W. Hung, M.-M. Lu, and S.-I. An, 2015: Linking emergence of the central Pacific El Niño to the Atlantic multidecadal oscillation. *J. Climate*, **28**, 651–662, doi:10.1175/JCLI-D-14-00347.1.

Yuan, X., 2004: ENSO-related impacts on Antarctic sea ice: A synthesis of phenomenon and mechanisms. *Antarct. Sci.*, **16**, 415–425, doi:10.1017/S0954102004002238.

——, and D. G. Martinson, 2001: The Antarctic dipole and its predictability. *Geophys. Res. Lett.*, **28**, 3609–3612, doi:10.1029/2001GL012969.

——, and C. Li, 2008: Climate modes in southern high latitudes and their impacts on Antarctic sea ice. *J. Geophys. Res.*, **113**, C06S91, doi:10.1029/2006JC004067.

Zamboni, L., F. Kucharski, and C. R. Mechoso, 2012: Seasonal variations of the links between the interannual variability of South America and the South Pacific. *Climate Dyn.*, **38**, 2115–2129, doi:10.1007/s00382-011-1116-z.

Zhou, T., and R. Yu, 2004: Sea-surface temperature induced variability of the Southern Annular Mode in an atmospheric general circulation model. *Geophys. Res. Lett.*, **31**, L24206, doi:10.1029/2004GL021473.

Zubiaurre, I., and N. Calvo, 2012: The El Niño–Southern Oscillation (ENSO) Modoki signal in the stratosphere. *J. Geophys. Res.*, **117**, D04104, doi:10.1029/2011JD016690.